# The Kinetics of Mechanically Coupled Myosins Exhibit Group Size-Dependent Regimes

Lennart Hilbert,[†††‡‡] Shivaram Cumarasamy,[‡‡] Nedjma B. Zitouni,[‡‡] Michael C. Mackey,[†‡§††] and Anne-Marie Lauzon[†¶‖‡‡*]

Departments of [†]Physiology, [‡]Mathematics, [§]Physics, [¶]Medicine, and [‖]Biomedical Engineering; [††]Centre for Applied Mathematics in Bioscience and Medicine, and [‡‡]Meakins-Christie Laboratories, McGill University, Montréal, Québec, Canada

ABSTRACT Naturally occurring groups of muscle myosin behave differently from individual myosins or small groups commonly assayed in vitro. Here, we investigate the emergence of myosin group behavior with increasing myosin group size. Assuming the number of myosin binding sites ($N$) is proportional to actin length ($L$) ($N = L/35.5$ nm), we resolve in vitro motility of actin propelled by skeletal muscle myosin for $L = 0.2$–$3$ $\mu$m. Three distinct regimes were found: $L < 0.3$ $\mu$m, sliding arrest; $0.3$ $\mu$m $\leq L \leq 1$ $\mu$m, alternation between arrest and continuous sliding; $L > 1$ $\mu$m, continuous sliding. We theoretically investigated the myosin group kinetics with mechanical coupling via actin. We find rapid actin sliding steps driven by power-stroke cascades supported by postpower-stroke myosins, and phases without actin sliding caused by prepower-stroke myosin buildup. The three regimes are explained: $N = 8$, rare cascades; $N = 15$, cascade bursts; $N = 35$, continuous cascading. Two saddle-node bifurcations occur for increasing $N$ (mono → bi → mono-stability), with steady states corresponding to arrest and continuous cascading. The experimentally measured dependence of actin sliding statistics on $L$ and myosin concentration is correctly predicted.

## INTRODUCTION

It is widely believed that the relative sliding of actin and myosin filaments, driven by groups of myosin protein motors pulling on actin, is the basic mechanism of muscle contraction. However, the most detailed knowledge of this mechanism is gained from laser trap studies, which investigate the in vitro molecular mechanics of single or a few myosin molecules' interactions with a single actin filament. It has been found that the effect larger groups of myosin exert on a single actin filament can differ significantly, e.g., the actin sliding velocity in the in vitro motility assays exceeds expectations from single myosin studies up to twofold (1,2). It was deduced that this augmentation results from cooperativity between individual myosins that is established by mechanical coupling via the jointly propelled actin filament (1–4).

The interaction of a single myosin with actin can be described as a mechanochemical cycle that couples hydrolysis of adenosine triphosphate to myosin conformational changes that propel actin (5,6). Two mechanical steps occur during one mechanochemical cycle: the main power stroke transition (power-stroke step size $d = 4$ nm), and a minor mechanical transition (predetachment step size $d = 2$ nm) that precedes myosin detachment from actin (7). Accordingly, actin's myosin binding sites can be in one of three distinct kinetic states at any given time: bound by myosin before its fast main power stroke (prepower stroke), bound by myosin after its main power stroke (postpower stroke), or not bound by myosin (unbound). The rate of the detachment step is strain-dependent in smooth muscle myosin: a retarding load slows down detachment and a supporting load accelerates it (8,9). The same strain-sensitivity of detachment has been hypothesized to be present in skeletal muscle myosin (10,11). The reasoning is that work has to be exerted when mechanical transitions occur under load, which alters the reaction's energetics and in turn the reaction rate. By this logic, the rates of both the main power stroke and the predetachment step in skeletal muscle myosin should be strain-dependent.

Strain-dependent detachment kinetics, in combination with mechanical coupling via a jointly propelled actin filament, was proposed as a mechanism of accelerated actin sliding (2–4). Such coupling can, however, give rise to additional macroscopic behaviors (12,13). For actomyosin interactions, complex behavior was observed near loads constituting isometric force ($F_{max}$) (12,14–18). In the two-headed myosin V cellular cargo transport motor, strain-sensitive protein motor kinetics have been identified as the crucial mechanism underlying coordinated stepping of the two heads (19–22). There, single motors act as loads on other single motors' strain-dependent kinetics, and no external loads are required to elicit the behavior that emerges for a group of motors. Further, motility assays using different ratios of slow and fast myosin have shown that interactions between myosin motors working on the same actin filament lead to nonlinear interactions between fast and slow myosin kinetics (23,24).

In this study, we use an in vitro motility assay of actin filaments propelled by skeletal muscle myosin to investigate how the group behavior exhibited by mechanically coupled

*Submitted April 2, 2013, and accepted for publication July 29, 2013.*

*Correspondence: anne.lauzon@mcgill.ca

Editor: Claudia Veigel.



0006-3495/13/09/1466/9 $2.00

http://dx.doi.org/10.1016/j.bpj.2013.07.054

myosins emerges as the number of coupled myosins increases. Given the proportionality of the number of myosin binding sites to actin length ($L$) (7,25), we employ newly developed software to analyze motility assay videos and resolve the results by $L$. Further, we develop three mathematical models of the mechano-chemistry of the interaction of myosin with myosin binding sites on actin. A detailed stochastic mechanical model is used to explain the most striking experimental observations and justify a simplified continuous model and its stochastic implementation for further explanation of our experimental observations.

## METHODS

### Protein purification

Skeletal muscle myosin was purified from chicken pectoralis muscle as in Sobieszek's protocol (26) with a modified extraction buffer ([KCl] = 0.5 M). Actin filaments were purified from chicken pectoralis acetone powder (27) and stored at 4°C. Actin was fluorescently labeled by incubation with tetramethylrhodamine isothiocyanate-labeled phalloidin (Sigma-Aldrich, St. Louis, MO) (24).

### In vitro motility assay

Nonfunctional myosin heads were removed by ultracentrifugation (TLA-42.2 rotor in an Optima L-90K ultracentrifuge; Beckman Coulter, Fullerton, CA) and flow-through chambers and buffers were prepared and used as previously described by Léguillette et al. (28). The oxygen scavenger contained 0.16 mg/mL glucose oxidase, 0.045 mg/mL catalase, and 5.75 mg/mL glucose. Before incubation in the flow-through chamber, myosin at a concentration of 0.5 mg/mL was diluted by addition of myosin buffer (see Table 1).

### Video recording

Actin motility was visualized using an inverted microscope (IX70; Olympus, Melville, NY), recorded with an image-intensified charge-coupled device camera (KP-E500, 30 fps; Hitachi, Chiyoda, Tokyo, Japan), and digitized with a custom-built computer (Norbec Communication, Montréal, Québec, Canada).

### Video analysis

Custom-written MATLAB software (The MathWorks, Natick, MA) was used for analysis of actin filament motion. Contrast was enhanced by averaging every three consecutive video frames, giving an effective time resolution of 100 ms. Image frames were thresholded into binary black-and-white images. Filament images were extracted using the MATLAB Image Processing Toolbox's Connected Components function and tracked based on similarity of area and centroid. The frame-to-frame velocity ($V_{f2f}$) was calculated by dividing the distance between a filament's centroid position (center of mass from grayscale pixel values) in two consecutive frames by the time resolution of $\Delta t = 0.1$ s. $V_{f2f}$ was used where a fixed observation time across all measured velocities was desirable. The trace velocity ($v$) was determined by tracking the length of the path traveled by the leading tip of a filament, and dividing by the time of observation of the filament ($T$). The trace velocity avoids the centroid method's bias to underestimate the velocity for longer filaments due to the centroid exhibiting a "cutting corners" behavior during filament turning (29), and was used where unbiased, quantitative accuracy for longer filaments was desirable. The trace velocities as well as the filament length were determined using a transformation of images of elongated objects into rectangles of equal perimeter and area, with the longer edge representing the object length (30).

**TABLE 1 Overview of recorded motility data**

| Dilution[a] | Final [My] | $n$ Flow-through chambers |
|---|---|---|
| 1/4 | 0.125 mg/mL | 16 |
| 1/5 | 0.100 mg/mL | 16 |
| 1/7 | 0.071 mg/mL | 8 |
| 1/9 | 0.056 mg/mL | 8 |

[a]Fraction of 0.5 mg/mL myosin preparation in assay buffer.

### Statistical analysis

95% bootstrap confidence intervals (2500 resamples) were used. Statistical significance ($p < 0.05$) is indicated by confidence intervals not overlapping 0.

## EXPERIMENTAL RESULTS

Below $L \approx 0.3$ $\mu$m, all analyzed actin filaments are in a nonmotile state: there is no motion other than random fluctuations around a fixed position on the motility surface (Fig. 1, *A* and *B*). Above $L \approx 0.3$ $\mu$m, filaments switched between the nonmotile state and a motile state of directed motion. For increasing $L$ beyond 0.3 $\mu$m, a decreasing number of filaments move at intermediate velocities (Fig. 1, *A* and *B*). The velocity of the motile state increased with actin length (Fig. 1 *C*). Below $L \approx 1$ $\mu$m the motile fraction ($f_{mot}$) linearly ascends to a plateau value close to 1, and above $L \approx 1$ $\mu$m remains at this plateau value. This indicates that $L \approx 1$ $\mu$m is a qualitative separating point between actin that is sufficiently long to support continuous, uninterrupted sliding motion, and actin that is too short to do so. In summary, there are three actin-length-dependent regimes of actin sliding behavior: below $L \approx 0.3$ $\mu$m, actin filaments are persistently arrested to the motility surface (nonmotile state); between $L \approx 0.3$ $\mu$m and $L \approx 1$ $\mu$m, actin filaments discretely switch between the nonmotile and the motile state; and above $L \approx 1$ $\mu$m, the motile state is observed almost exclusively.

Lowering the myosin concentration ([My]) lowered the velocity of the motile state and led to a slower increase of this velocity with increasing $L$ (Fig. 1 *D*). The critical length ($L_c$, the length above which $f_{mot}$ has attained a plateau value) was statistically significantly increased for [My] = 0.056 mg/mL when compared to [My] = 0.125 mg/mL (Fig. 2, *A–C*). At a given $L$, a lower [My] can be assumed to result in a lower number of myosins being simultaneously bound to the actin filament. This result indicates that the number of simultaneously bound myosin motors, and not primarily $L$, is the parameter determining the transition from mixed to persistently motile actin sliding (31).

As discussed earlier, above $L_c$, actin has attained a plateau in $f_{mot}$. Therefore, above $L_c$, the mean actin sliding velocity is not influenced by the amount of time actin spends in a stopped state. However, for [My] = 0.125 mg/mL, we

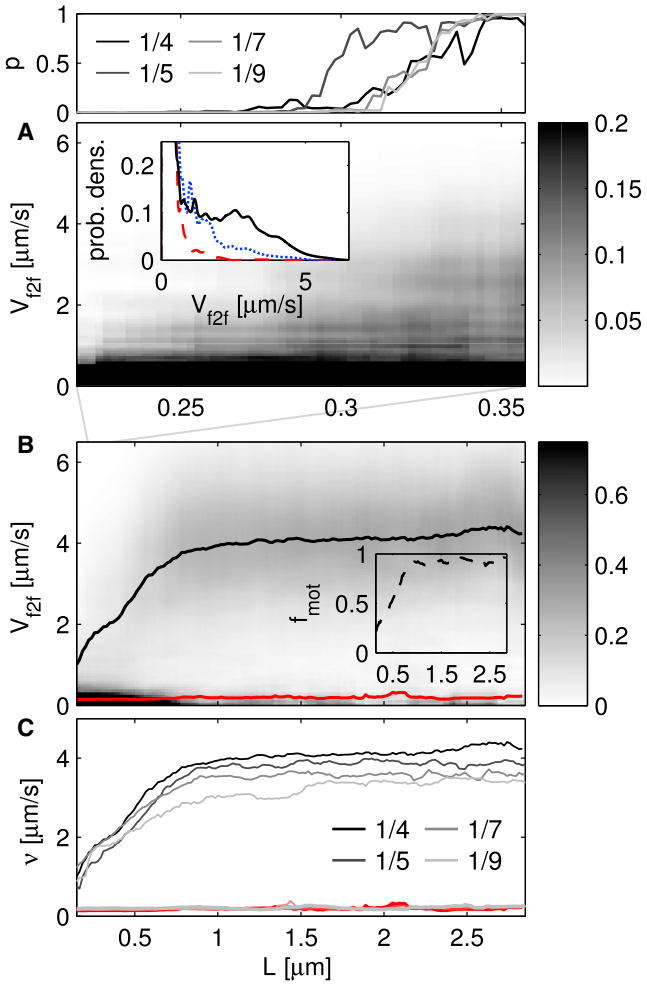


FIGURE 1 Experimental detection of the three regimes of actin sliding. (*A*) (*Main panel*) Histograms of frame-to-frame velocities of actin sliding ($V_{f2f}$) determined across a range of actin filament length ($L$) for [My] = 0.125 mg/mL. (*Inset*) Empirical $V_{f2f}$ probability distributions in specific $L$ ranges (*dashed red*, *dotted blue*, and *solid black lines* represent $L \in$ [0, 0.26], [0.29, 0.31], and [0.325, 0.4] $\mu$m, respectively), indicating that below $L \approx 0.3$ $\mu$m only a single mode of $V_{f2f}$ is visible. (*Small top panel*) The Dip Test $p$ value ($p < 0.05$ suggests unimodality) further indicates that only a single mode exists in the $V_{f2f}$ distribution below $L \approx 0.3$ $\mu$m (50). This single mode observed below $L \approx 0.3$ $\mu$m corresponds to actin that is fully arrested to the motility surface (see Fig. S1 in the Supporting Material). (*B*) Main panel as in panel *A*, except for a different $L$ range. (*Solid lines*) Means of a two-Gaussian mixture model that was fitted to the $V_{f2f}$ distribution. (*Inset*) Up to $L \approx 1$ $\mu$m, the fraction of sliding motion associated with the motile state (motile fraction, $f_{mot}$) linearly increases up to $f_{mot} \approx 1$, indicating a characteristic length at which continuous actin sliding is established. (*C*) Two-Gaussian mixture model means as shown in panel *B*, but determined for the four different [My] values used in our experiments. Lowering [My] value reduces the maximally attained velocity of the motile state. Sliding window parameters: (*A*) $L_{min} = 0.175$ $\mu$m, $L_{max} = 0.4$ $\mu$m, window width 0.019 $\mu$m, 60 windows; (*B* and *C*) $L_{min} = 0$ $\mu$m, $L_{max} = 3.0$ $\mu$m, window width 0.3 $\mu$m, 150 windows.

observed a statistically significant increase in the mean sliding velocity $v$ even above $L_c$ (Fig. 2 *D*). In prior studies, $v$ increases with $L$ were explained by phases in which no myosin is bound to actin and therefore actin is not propelled (32,33). Here, however, actin is consistently propelled for $L > L_c$, but $v$ still increases. This indicates that above $L_c$, there are always myosins attached to actin, whereas a further increase of the number of myosins simultaneously attached to actin leads to a further $v$ increase. At lower [My], this group effect is lost, possibly indicating that a minimal [My] is necessary for this inter-myosin effect (Fig. 2, *E* and *F*).

Although the stop-and-go motion in the intermediate regime is visible at timescales of hundreds of milliseconds to seconds, the common molecular level explanation—the temporary unavailability of myosin to propel actin—should take place on a much smaller timescale of tens of milliseconds (32,33). We investigated this discrepancy based on fluctuations in the velocity. The coefficient of variation (standard deviation $\sigma_v$ over mean $\mu_v$) gives a nondimensional measure of fluctuation strength. Further, for a sufficiently large sample of $N_v$ independent positive measurements, the Law of Large Numbers states $\sigma_v/\mu_v \propto {N_v}^{-1/2}$. To scale out $N_v$ influence, we defined the scaled deviation as $\delta_v = (\sigma_v/\mu_v)\sqrt{N_v}$. We assume that the measured velocities result from underlying actin-myosin interactions: if myosin binding sites are independent, then $N_v \propto L$; if the average rate of actin-myosin interactions is stationary over the time of observation $T$, then $N_v \propto T$. In this hypothetical situation, we would expect

$$\delta v = \frac{\sigma_v}{\mu_v}\sqrt{\frac{LT}{(1\ \mu\text{m s})}} = \text{const.} \qquad (1)$$

across all $L$. In contrast, an increase in $\delta v$ indicates a decrease in the degree of independence (stronger correlation between interaction events) or a slowing down of kinetics. A decrease in $\delta v$ indicates an increased independence (decreased correlation between interaction events) or an acceleration of kinetics.

The value $\delta v$ exhibits a nontrivial $L$ and [My] dependence. For all [My], starting from lowest $L$, we observed an initial $\delta v$ increase up to a maximum close to $L \approx 0.3$ $\mu$m (Fig. 2, *G* and *H*). This coincides closely with the $L$ value at which the motile state first emerges (Fig. 1, *A* and *B*). Then, for [My] = 0.0125, 0.100, 0.071 mg/mL, but not for [My] = 0.052 mg/mL, $\delta v$ drops to a minimum at $L \approx 1$ $\mu$m (Fig. 2, *G* and *H*). This minimum coincides closely with the attainment of consistent sliding motion (Fig. 1 *B*, *inset*). All features seemed sufficiently clear to not require statistical testing, except for the increase in $\delta v$ following the minimum at $L \approx 1$ $\mu$m, which upon testing does reach statistical significance for the [My] exhibiting a minimum (Fig. 2 *I*).

Considering $V_{f2f}$, $f_{mot}$, $v$, and $\delta v$ observations, we suggest the following interpretation of the three regimes of actin sliding:

1. Below $L \approx 0.3$ $\mu$m, actin sliding is fully arrested, whereas myosins are still acting as cross-linkers preventing actin from floating away from the motility surface.

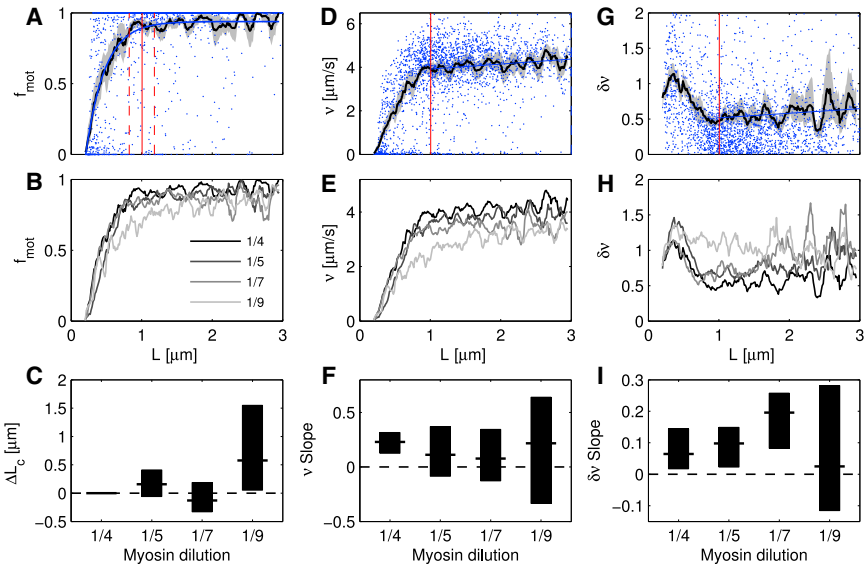


FIGURE 2 Quantitative features of actin sliding. (*A*) $f_{mot}$, quantified as fraction of $V_{f2f}$ above threshold velocity $V_{thr} = 1.0\ \mu m\ s^{-1}$. (*Blue dots*) Single filament $f_{mot}$; (*thick black solid line*) sliding window average $F_{mot}$; (*thin blue solid line*) best fit (nonlinear least-squares) of $A(1-e^{-B(L-C)})$. (*A–C*) Free fitting parameters for adjustment to the sliding window average. (*Gray area*) 95% Bootstrap confidence interval. The critical length ($L_c$, *red vertical line*; 95% bootstrap confidence interval, *dashed lines*) was determined as the point where the fitted $F_{mot}(L)$ function reached $0.95 \cdot A$, indicating that the $f_{mot}$ plateau identified in Fig. 1 *C* (*inset*) was attained. (*B*) As in panel *A* but for all values of [My], only sliding window average is shown. (For values of [My], see *inset*.) (*C*) $\Delta L_c$ differences (relative to [My] = 0.125 mg/mL), values are $\Delta L_c$ from the full data set for a given [My] with 95% bootstrap confidence intervals. (*D*) $v$, quantified as mean of trace velocities, with lines and symbols as in panel *A* (except for *black line*, linear fit to all shown single filament $v$ values above $L_c$). (*E*) As panel *D* for all values of [My], only sliding window average is shown (for values of [My], see *inset* in panel *B*). (*F*) Slopes of linear fit to $v$ for $L \geq L_c$. (*G*) $\delta v$, Lines and symbols as in panel *A* (except *black line*, linear fit to $\delta v$ values above $L_c$). (*H*) As in panel *G* for all values of [My], only sliding window average is shown (for values of [My], see *inset* in panel *B*). (*I*) Slopes of linear fit to $\delta v$ for $L \geq L_c$. Sliding window parameters for all length-resolved plots: $L_{min} = 0.15\ \mu m$, $L_{max} = 3.0\ \mu m$, window width 0.10 $\mu$m, 200 windows. Note that differences from 0 were assumed statistically significant ($p < 0.045$) where confidence intervals did not overlap with 0.

This indicates that the completion of full actin-myosin interaction cycles is slowed down or fully stopped. All fluctuations in $v$ result from random fluctuations around the fixed position of the actin filaments. For increasing $L$, a second, motile state occurs, which introduces slow jumping between full arrest and a discrete, but very slow, motile state. This slow jumping leads to the observation of several consequent instantaneous velocities in either the arrested or the motile state—highly correlated, consecutive sliding velocities, which lead to an increase in $\delta v$.

2. Between $L \approx 0.3\ \mu m$ and $L \approx 1\ \mu m$, the velocity of the motile state as well as the fraction of overall observation time that filaments spend in the motile state increase with $L$. Thus, the rate at which actin-myosin interaction cycles are completed while in the motile state, as well as the time spent in this motile state, increase with $L$. Both factors accelerate the gross rate of completion of actin-myosin interactions, which reduces $\delta v$.
3. Above $L \approx 1\ \mu m$, almost all of the observation time is spent in the motile state, and either an increase or no statistically significant change in the velocity of the motile state is observed—these observations by themselves would warrant either a further decrease or, more likely, a constant level of $\delta v$. However, an increase of $\delta v$ is observed. This indicates that increasing $L$ beyond $L \approx 1\ \mu m$ no longer increases the effective sample size of actin-myosin interactions that result in the measured sliding velocities. This would be explicable by a situation where all myosins that are simultaneously bound to an actin filament are maximally mechanically coupled, and thus effectively appear as a completely integrated macroscopic system. Such a system's dynamics would become effectively independent of the system's constituent parts, and thus not change fundamentally anymore, even when the number of parts increases.

## MATHEMATICAL MODELS

### Mechanistic explanation of nonmotile and motile state

We constructed three mathematical models, all resting on the assumption that the number of myosin binding sites on an actin filament ($N$) is proportional to the length of the actin filament ($L$). We assume a distance of 35.5 nm between major binding sites (7,25). Our first model monitors stochastic changes in the chemical as well as the mechanical state of the individual myosin binding sites located on the same actin filament. A unidirectional three-state chemical cycle (unbound → prepower-stroke → postpower-stroke → unbound) was assumed (7,8). Chemical reactions take place at discrete time points, after which the overall actin-myosin system immediately relaxes to a force equilibrium. Myosins bound to a binding site on actin were assumed to have an unstrained position, and a linear force response when being moved away from that position. The rates of both the main power stroke and a minor power stroke preceding the detachment depend on the mechanical work that would have to be exerted on all myosins currently bound to the actin filament to execute the mechanical transition (1–3,8). (See also Fig. 3 *A* and the Supporting Material.)

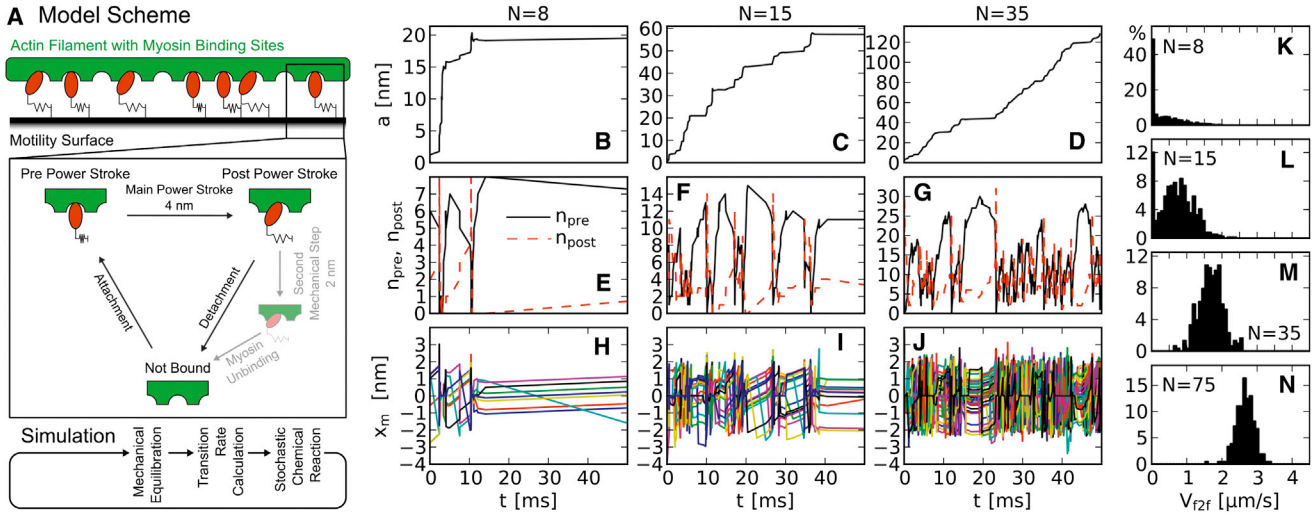


FIGURE 3 Description and results of the detailed stochastic mechanical model. (*A*) Model description: Due to its helical form, binding sites are placed equidistantly along the actin filament (helical symmetry at 35.5 nm) (7,25) leading to a proportionality of $L$ and the number of binding sites ($N$). Each myosin binding site with a myosin bound is assumed to exhibit a linear force response to displacement from its unstrained position. A unidirectional three-state kinetic scheme is used, where the main power stroke is 4 nm long; myosin detachment is conditional on the prior occurrence of a second minor power stroke of 2 nm, after which detachment immediately occurs due to adenosine triphosphate saturation in the motility buffer (7,8). For both mechanical transitions, the rate is dependent on the mechanical work that has to be exerted to adjust the overall actin-myosin mechanical network to the changes inflicted by this step (1–3,8). The iteration scheme for simulation is shown in the bottom of the panel. (*B–J*) Example filament sliding distances (*B–D*), post and prepower-stroke binding site counts (*E–G*), and individual myosins' displacements from the unstrained position (*H–J*) for different $N$, as indicated above panels (values drawn for every chemical reaction). (*K–N*) Histograms of $V_{f2f}$ (sampled at the time resolution used in experiment, $\Delta t = 0.1$ s) for different $N$ as indicated in the panels (bin height is a bin's percentage of the sum of all bins' counts).

Our stochastic simulation, unlike commonly used Euler-type schemes with equal time steps, iterates from one chemical reaction to the next. This results in an exact time resolution for all transitions in the system, and inherently circumvents problems of methods approximating continuous processes by finite time differences. We observe that actin sliding occurs in rapid steps, which are interspersed in between longer phases without actin motion (Fig. 3, *B–D*). For increasing $N$, the frequency of these steps increases and the phases without motion become shorter, which leads to an average acceleration of actin sliding. The rapid steps in actin sliding coincide with cascades in the transition of myosin binding site chemical states (Fig. 3, *E–G*). During phases without motion preceding an actin sliding step, myosin binding sites accumulate in the prepower-stroke state, until a rapid global transition into the postpower-stroke state and the unbound state occurs, which coincides with the rapid step in actin sliding. In terms of individual myosin strains, in phases preceding cascades, few Pre → Postpower-stroke transitions occur, which slowly build an increased strain on the remaining prepower-stroke state myosins (Fig. 3, *H–J*). The Pre → Post main power-stroke transition appears more frequently for higher $N$, which is due to strains being more homogeneously distributed across the range of strains; for low $N$, it is more likely that combinations of myosin strains occur that lead to a persistent block of Pre → Postpower-stroke transitions (see Movie S1 and Movie S2).

At intermediate $N$, cascades occur in bursts, which are a series of rapid consecutive cascades, or even overlap for high $N$ (Fig. 3, *D*, *G*, and *J*, and see Movie S3, Movie S4, Movie S5, Movie S6, Movie S7, and Movie S8).

When analyzed at $\Delta t = 0.1$ s, which we used for the analysis of our experiments, the $L$-dependent presence of a nonmotile and a motile state (Fig. 1, *A* and *B*) are reproduced (Fig. 3, *K–N*). The reproduction of the transient bimodal regime by the model despite the relatively coarse $\Delta t = 0.1$ is due to the grouping of cascades into bursts at intermediate $N$, causing a slow timescale stochastic alternation between nonmotile and motile phases (see Movie S9, Movie S10, and Movie S11).

## *N*-dependent saddle-node bifurcations

The detailed stochastic mechanical simulations indicated that the overall rate of the chemical reactions is accelerated by up to two orders of magnitude for an increased number of actin-bound postpower-stroke myosins, and decreased up to two orders of magnitude for an increased number of actin-bound prepower-stroke myosins (see Fig. S2 in the Supporting Material). Also, the myosin attachment to unbound binding sites was found as a rate-limiting step after the occurrence of a cascade, so that myosin detachment could be assumed as instantaneous and the postpower-stroke state and the unbound state could be joined into one state (see Fig. S3). Based on this, we formulated a simplified,

continuous model describing the dynamics of the fraction $n = (n_{post} + n_{unb})/N$ of the total binding sites that is not in the prepower-stroke state (for details, see the Supporting Material).

The simplified continuous model explains the three regimes of actin sliding behavior (nonmotile, intermittent motility, continuous motility) as a progression through two saddle-node bifurcations (mono → bi → mono-stability) for increasing $N$. The two stable steady states have the following properties (Fig. 4 *A, B*):

1. A large fraction of the myosin binding sites is in the prepower-stroke state, and the sliding velocity is $L \approx 0$.
2. A small fraction of the myosin binding sites in the prepower-stroke state, and the acting sliding velocity is clearly $>0$.

These properties suggest that the steady states are identifiable with:

1. The precascade phases in which actin is not sliding, and
2. The cascading phases during which actin slides.

This also indicates that the transitions from mono- to bimodal behavior in actin sliding indeed occur at critical $L$ associated with the saddle-node bifurcations.

The continuous model can further explain the dependence of the critical $L$ on [My] (Fig. 2 *C*), as the saddle node bifurcations occur at higher $N$ for lower [My] (Fig. 4 *B*). In addition, the reduced velocity of the motile population for lower [My] (Fig. 1 *C*) is captured (Fig. 4 *B*).

### Prediction of actin sliding statistics

Lastly, we derived a simplified stochastic simulation from our continuous model, which allowed us to sample $n$ and $a$ time courses (for details, see the Supporting Material, and Fig. 5). When sampled at $\Delta t = 0.1$ s, this simplified model also exhibits the $N$-dependent bimodality in $V_{f2f}$ that is observed in our experiments and the detailed stochastic mechanical model (Fig. 4 C). Further, this model correctly predicts the experimentally observed dependence of $f_{mot}$, $\nu$, and $\delta\nu$ on $N \propto L$ and [My]:

1. For all [My], $f_{mot}$ reaches a value close to 1; for lower [My], $f_{mot} = 1$ is only reached at greater $N \propto L$.
2. $\nu$ increases more slowly for lower [My]; $\nu$ still increases beyond the point where $f_{mot}$ has reached 95% of its plateau value (Fig. 5 *B*).
3. $\delta\nu$ follows the same qualitative pattern as in the experimentally determined statistics; the main peak quantitatively matches our experimental results, whereas away from the peak the overall values of $\delta\nu$ are smaller than in our experimental results (Fig. 5 *C*). This is likely due to additional sources of noise that are present in the experiment (see Fig. S1). However, the changes in $\delta\nu$ for lower [My] (shift of $\delta\nu$ peak location, loss of positive slope at high $N$) are predicted.

## DISCUSSION

Based on our experimental and theoretical findings, we suggest that the three regimes of actin sliding are defined by the existence or nonexistence of two global kinetic states and can be interpreted as follows (Fig. 6):

### Regime 1

Below $L \approx 0.3$ $\mu$m, actin filaments are permanently arrested to the motility surface. Nonfunctional myosin was removed from the assay (ultracentrifugation removal of nonfunctional myosin and blocking of nonfunctional myosins in the flow-through chamber by unlabeled actin), making permanent surface binding by nonfunctional myosin unlikely. Further, at least one myosin should be attached to actin at all times: the methylcellulose used in the motility buffer limits the lateral diffusion of actin; when no myosin is attached to actin, rapid longitudinal diffusion would occur (32). We did not observe such diffusion. Instead, as detailed by our mathematical models, perfectly functional myosins accumulate in the prepower-stroke state and mutually hinder each other's progression through the main power stroke, ultimately leading to a persistent self-blockade. The actin length of $L \approx 0.3$ $\mu$m is close to the diffraction limit for our fluorescent label ($L \approx 0.2$ $\mu$m), so the absolute value should be understood as an upper boundary for this regime.

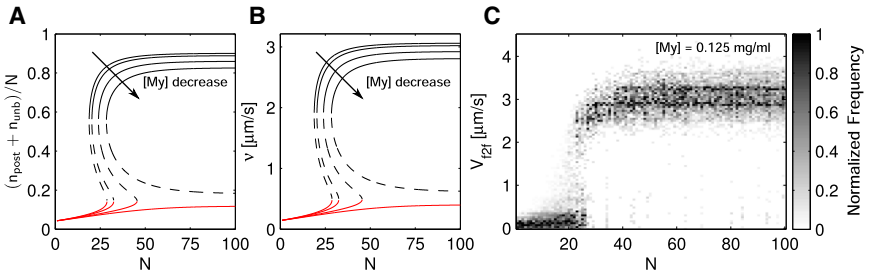


FIGURE 4 $N$ and [My]-dependent existence of the nonmotile and the motile configuration of the actin-myosin system. (*A* and *B*) The simplified deterministic model exhibits up to three steady states (*solid lines*, stable; *dashed line*, unstable) in $n_{post} + n_{unb}$ (*A*) which can be linked to sliding velocity predictions for experimentally observed actin sliding (*B*). (*Arrows*) Direction in which [My] is reduced, [My] = 0.125, 0.1, 0.072, 0.056 mg/mL were used, corresponding to our experiments. (*C*) $V_{f2f}$ distributions from the stochastic implementation of the simplified deterministic model (sampled at the time resolution used in experiment, $\Delta t = 0.1$ s). The two $N$-dependent populations correspond to the stable steady states.

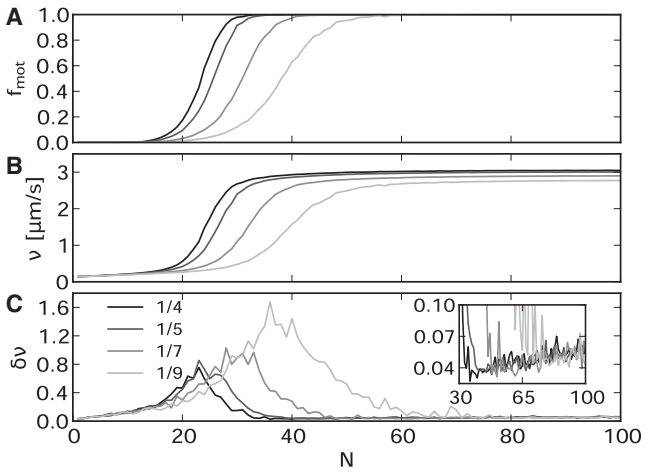


FIGURE 5 Theoretically predicted quantitative features of actin sliding. Shown are simulation results of the stochastic implementation of the simplified mathematical model of actin-myosin interactions. Five-hundred filaments were simulated at each $N$ value with 5000 iterations per myosin binding site, of which the first 3500 were removed to prevent bias from initial conditions. No sliding window averaging was applied; $V_{f2f}$ were sampled at time resolution of $\Delta t = 0.1$ s (corresponding to our experiments). For each $N$, the mean sliding velocity ($A$, arithmetic mean of $V_{f2f}$), the mean motile fraction ($B$, fraction of $V_{f2f} > V_{thr}$), and the scaled deviation ($C$, standard deviation of $V_{f2f}$ divided by arithmetic mean of $V_{f2f}$ and multiplied by $\sqrt{N}$) were determined. Panel $C$ (*inset*) demonstrates increasing prominence of the positive slope of $\delta v$ at high $N$ for higher [My]. The colors referring to [My] are given in the inset in panel $C$ for all panels.

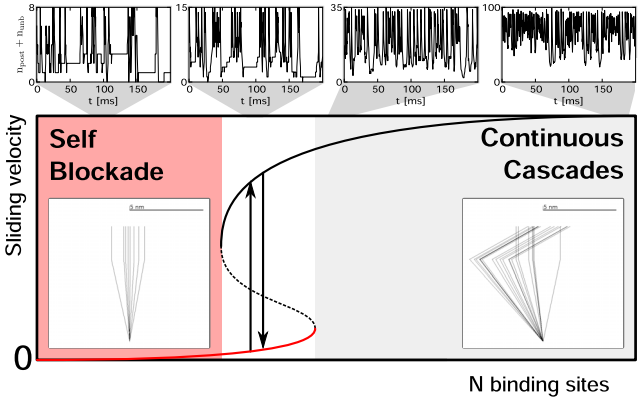


FIGURE 6 Three distinct, $N$-dependent regimes of actin sliding and underlying actin-myosin kinetics. (*Main panel*) Stable configurations of the overall actin-myosin network, which are attainable at a specific $N$. (*Red line*) Nonmotile, prepower-stroke dominated state. (*Black line*) Motile state without prepower-stroke buildup. For increasing $N$, occurrence and disappearance of these states akin to saddle-node bifurcations is observed. For intermediate $N$, a coexistence of both states is found, leading to the actin-myosin system stochastically alternating between the nonmotile and the motile state. (*Dashed black line*) Unstable steady state. (*Insets*) Example configurations of the actin-myosin system in the nonmotile (*left*, $N = 8$) and the motile regime (*right*, $N = 35$). Each line represents the displacement of a myosin bound to actin away from its unstrained position; prepower-stroke myosins have vertical top parts, postpower stroke myosins have angled top parts spanning 4 nm. (For examples of the dynamic behavior of the individual myosins, see Movie S1 and Movie S2 in the Supporting Material.) (*Small panels on top*) Example traces showing the dynamics of the number of myosin binding sites in the postpower-stroke and the unbound state ($n_{post} + n_{unb}$) for different $N$ (detailed stochastic model, $N$ indicated by the *topmost tick* on the *vertical axis* in each panel).

## Regime 2

Above $L \approx 0.3$ $\mu$m, actin sliding switches between the two discrete states of full arrest to the motility surface versus continuous forward sliding. It is unlikely that this is due to longitudinal diffusion during phases where actin is not bound to any myosin, because even shorter actin filaments with a lower chance of not binding a myosin did not exhibit such diffusion behavior. Rather, as detailed by our mathematical models, the entire group of myosins simultaneously bound to actin dynamically switches between two group states: nonmotile and motile. The motile state is driven by bursts of cascades, during which the main power-stroke transition is supported by postpower-stroke myosins. At $L \approx 1.0$ $\mu$m, the motile state fully dominates, and actin slides continuously at almost all times. This level of continuous sliding is attained in a linear fashion for increasing $L$, where continuous motion is established rather sharply at $L \approx 1.0$ $\mu$m. This length of full continuous sliding increases for lowered [My], indicating that a critical group size, and not a critical actin length, is necessary for continuous performance of the myosin motor group.

## Regime 3

Above this critical group size, continuous actin sliding (full sustained motility) is established, driven by an unbroken sequence of cascades, meaning a permanent support of the main power stroke by postpower-stroke myosins. For [My] = 0.125 mg/mL, the sliding velocity keeps increasing with increasing actin length. This indicates that a further increase in the myosin group size can indeed lead to a further increase in the rate of detachment of myosin from the actin filament, which is also indicated by our mathematical models.

## Concluding remarks

Our modeling approach could be extended by:

1. Explicit treatment of the nonbound state in the continuous model analysis;
2. The inclusion of nonlinear elasticity of myosin (34); or
3. Including possible interactions between the two motor heads of myosin (35).

Actin-length-resolved analysis of motility assay data have been used in earlier studies (32,33), and the switching between a nonmotile and a motile state of motility has been studied by Marston and co-workers (36–39) characterizing actin regulatory proteins. To our knowledge, however, both aspects have not been investigated simultaneously before. Thus, existent mathematical models of

actin-length-dependent changes only deal with average sliding velocities, but not with a bimodality between a nonmotile and a motile state (4,32,33). Also, these mathematical models cannot explain how actin sliding velocity keeps increasing when a plateau in the motile fraction has already been reached (Fig. 2, *D–F*) (32,33).

Although it is intuitively clear that a group behavior must emerge as the group size is increased, most experimental studies tackle either small (around 5–8 coupled motors) (12,22,31,40–47) or large (100 or more motors) motor groups (4,12,14–18). Most studies investigate one specific group size rather than the dependence of group behavior on group size. Some investigate within a range of up to $\pm 3$ motors. Effectively, the middle ground (10–100 coupled motors), where myosin group behavior emerges, is left out. Note, however, the work of Badoual et al. (48), Uyeda et al. (32), Harris and Warshaw (33), Li et al. (49), and Kaya and Higuchi (34). Our study demonstrates and conceptualizes the emergence of a group behavior, starting from a group size of $N \approx 10$ coupled myosin binding sites, which actually seems to be a hindrance to the group's performance, and progresses up to $N \approx 100$ binding sites, thus capturing the establishment of full group behavior.

Debold et al. (47) have executed laser trap (tri-bead) assays with $N \approx 8$ motors being in the binding range of an individual $L \approx 0.5$ $\mu$m actin filament at the same time. In contrast to our experiments, the actin filament was readily and continuously moved at this group size. Compared to our experiments, a slower binding of myosin to free binding sites can be expected. Their myosin concentration of 15 $\mu$g/mL is almost one-tenth what we used, and the presentation of myosin on a pedestal is a geometry that brings less myosin-coated surface near the actin filament. Indeed, reducing $k_a$ in our detailed stochastic mechanical simulation leads to a significant reduction of actin sliding arrest (see Fig. S4). Thus, $k_a$ differences might explain the different observations between our studies. Kaya and Higuchi (34) investigated the in vitro interaction of actin with myosin-myorod filaments. Actin sliding in their assays happened in a stepwise fashion, with unloaded sliding velocities of 0.2–0.5 $\mu$m/s. Due to the myosin-myorod preparation, few myosins ($N \approx 5$) interact with actin, which again would suggest a lowered $k_a$, so that sliding arrest is reduced (see Fig. S4).

Badoual et al. (48) theoretically investigated bidirectional in vitro sliding behavior in terms of motor group size, and the predicted behavior could be confirmed in an in vitro system using engineered motors working in opposite directions. We detected bimodal motile/nonmotile behavior in a unidirectional, unengineered motor system. This indicates that a physiologically relevant skeletal muscle myosin motor cooperativity mechanism exists. This cooperativity mechanism collapses at unusually small motor group sizes, thus allowing us to understand its detailed workings.

## SUPPORTING MATERIAL

Four figures, and eleven movies are available at http://www.biophysj.org/biophysj/supplemental/S0006-3495(13)00913-2.

We thank Josh E. Baker, Genevieve Bates, Gijs Ijpma, Del R. Jackson, Jinzhi Lei, Oleg S. Matusovsky, Horia N. Roman, and Romain Yvinec for discussions, and Marvid Poultry for the procurement of the chicken breasts for the purification of skeletal muscle actin. We also thank the anonymous reviewers for their suggestions. The Colosse super computer of the CLUMEQ consortium was used for some of the stochastic simulations.

We acknowledge funding from the National Sciences and Engineering Council of Canada under grants No. 217457 and No. 224631. The Meakins-Christie Laboratories, Research Institute of the McGill University Health Centre, are supported in part by a Centre grant from Le Fonds de la Recherche en Santé du Québec. L.H. was supported by the McGill University Health Centre Research Institute Graduate Fellowship and the Centre for Applied Mathematics in Biosciences and Medicine Graduate Fellowship.

## REFERENCES

1. Baker, J. E., C. Brosseau, …, D. M. Warshaw. 2002. The biochemical kinetics underlying actin movement generated by one and many skeletal muscle myosin molecules. *Biophys. J.* 82:2134–2147.
2. Baker, J. E., C. Brosseau, …, D. M. Warshaw. 2003. The unique properties of tonic smooth muscle emerge from intrinsic as well as intermolecular behaviors of myosin molecules. *J. Biol. Chem.* 278:28533–28539.
3. Jackson, Jr., D. R., and J. E. Baker. 2009. The energetics of allosteric regulation of ADP release from myosin heads. *Phys. Chem. Chem. Phys.* 11:4808–4814.
4. Walcott, S., D. M. Warshaw, and E. P. Debold. 2012. Mechanical coupling between myosin molecules causes differences between ensemble and single-molecule measurements. *Biophys. J.* 103:501–510.
5. Huxley, A. F., and R. M. Simmons. 1971. Proposed mechanism of force generation in striated muscle. *Nature.* 233:533–538.
6. Eisenberg, E., T. L. Hill, and Y. Chen. 1980. Cross-bridge model of muscle contraction. Quantitative analysis. *Biophys. J.* 29:195–227.
7. Capitanio, M., M. Canepari, …, R. Bottinelli. 2006. Two independent mechanical events in the interaction cycle of skeletal muscle myosin with actin. *Proc. Natl. Acad. Sci. USA.* 103:87–92.
8. Veigel, C., J. E. Molloy, …, J. Kendrick-Jones. 2003. Load-dependent kinetics of force production by smooth muscle myosin measured with optical tweezers. *Nat. Cell Biol.* 5:980–986.
9. Kad, N. M., J. B. Patlak, …, D. M. Warshaw. 2007. Mutation of a conserved glycine in the SH1-SH2 helix affects the load-dependent kinetics of myosin. *Biophys. J.* 92:1623–1631.
10. Nyitrai, M., and M. Geeves. 2004. Adenosine diphosphate and strain sensitivity in myosin motors. *Philos. Trans. Roy. Soc. B. Biol. Sci.* 359:1867–1877.
11. Minozzo, F. C., L. Hilbert, and D. E. Rassier. 2012. Pre-power-stroke cross-bridges contribute to force transients during imposed shortening in isolated muscle fibers. *PLoS ONE.* 7:e29356.
12. Guérin, T., J. Prost, …, J.-F. Joanny. 2010. Coordination and collective properties of molecular motors: theory. *Curr. Opin. Cell Biol.* 22:14–20.
13. Duke, T. 2002. Push or pull? Teams of motor proteins have it both ways. *Proc. Natl. Acad. Sci. USA.* 99:6521–6523.
14. Duke, T. A. 1999. Molecular model of muscle contraction. *Proc. Natl. Acad. Sci. USA.* 96:2770–2775.

15. Duke, T. 2000. Cooperativity of myosin molecules through strain-dependent chemistry. *Philos. Trans. Roy. Soc. B. Biol. Sci.* 355:529–538.

16. Vilfan, A., and T. Duke. 2003. Instabilities in the transient response of muscle. *Biophys. J.* 85:818–827.

17. Riveline, D., A. Ott, …, J. Prost. 1998. Acting on actin: the electric motility assay. *Eur. Biophys. J.* 27:403–408.

18. Plaçais, P. Y., M. Balland, …, P. Martin. 2009. Spontaneous oscillations of a minimal actomyosin system under elastic loading. *Phys. Rev. Lett.* 103:158102.

19. Baker, J. E., E. B. Krementsova, …, D. M. Warshaw. 2004. Myosin V processivity: multiple kinetic pathways for head-to-head coordination. *Proc. Natl. Acad. Sci. USA.* 101:5542–5546.

20. Purcell, T. J., H. L. Sweeney, and J. A. Spudich. 2005. A force-dependent state controls the coordination of processive myosin V. *Proc. Natl. Acad. Sci. USA.* 102:13873–13878.

21. Craig, E. M., and H. Linke. 2009. Mechanochemical model for myosin V. *Proc. Natl. Acad. Sci. USA.* 106:18261–18266.

22. Lu, H., G. G. Kennedy, …, K. M. Trybus. 2010. Simultaneous observation of tail and head movements of myosin V during processive motion. *J. Biol. Chem.* 285:42068–42074.

23. Harris, D. E., S. S. Work, …, D. M. Warshaw. 1994. Smooth, cardiac and skeletal muscle myosin force and motion generation assessed by cross-bridge mechanical interactions in vitro. *J. Muscle Res. Cell Motil.* 15:11–19.

24. Warshaw, D. M., J. M. Desrosiers, …, K. M. Trybus. 1990. Smooth muscle myosin cross-bridge interactions modulate actin filament sliding velocity in vitro. *J. Cell Biol.* 111:453–463.

25. Steffen, W., D. Smith, …, J. Sleep. 2001. Mapping the actin filament with myosin. *Proc. Natl. Acad. Sci. USA.* 98:14949–14954.

26. Sobieszek, A. 1994. Smooth Muscle Myosin: Molecule Conformation, Filament Assembly and Associated Regulatory Enzymes. Birkhauser, Basel, Switzerland Chapt. 1, 1–29.

27. Pardee, J. D., and J. A. Spudich. 1982. Purification of muscle actin. *Methods Enzymol.* 85(Pt B):164–181.

28. Léguillette, R., N. B. Zitouni, …, A.-M. Lauzon. 2008. Affinity for MgADP and force of unbinding from actin of myosin purified from tonic and phasic smooth muscle. *Am. J. Physiol. Cell Physiol.* 295:C653–C660.

29. Work, S. S., and D. M. Warshaw. 1992. Computer-assisted tracking of actin filament motility. *Anal. Biochem.* 202:275–285.

30. Root, D., and K. Wang. 1994. Calmodulin-sensitive interactions of human nebulin fragments with actin and myosin. *Biochemistry.* 33:12581–12591.

31. Furuta, K., A. Furuta, …, H. Kojima. 2013. Measuring collective transport by defined numbers of processive and nonprocessive kinesin motors. *Proc. Natl. Acad. Sci. USA.* 110:501–506.

32. Uyeda, T. Q., S. J. Kron, and J. A. Spudich. 1990. Myosin step size. Estimation from slow sliding movement of actin over low densities of heavy meromyosin. *J. Mol. Biol.* 214:699–710.

33. Harris, D. E., and D. M. Warshaw. 1993. Smooth and skeletal muscle myosin both exhibit low duty cycles at zero load in vitro. *J. Biol. Chem.* 268:14764–14768.

34. Kaya, M., and H. Higuchi. 2010. Nonlinear elasticity and an 8-nm working stroke of single myosin molecules in myofilaments. *Science.* 329:686–689.

35. Albet-Torres, N., M. J. Bloemink, …, A. Månsson. 2009. Drug effect unveils inter-head cooperativity and strain-dependent ADP release in fast skeletal actomyosin. *J. Biol. Chem.* 284:22926–22937.

36. Marston, S. 2003. Random walks with thin filaments: application of in vitro motility assay to the study of actomyosin regulation. *J. Muscle Res. Cell Motil.* 24:149–156.

37. Fraser, I. D., and S. B. Marston. 1995. In vitro motility analysis of smooth muscle caldesmon control of actin-tropomyosin filament movement. *J. Biol. Chem.* 270:19688–19693.

38. Fraser, I. D., and S. B. Marston. 1995. In vitro motility analysis of actin-tropomyosin regulation by troponin and calcium. The thin filament is switched as a single cooperative unit. *J. Biol. Chem.* 270:7836–7841.

39. Bing, W., I. D. Fraser, and S. B. Marston. 1997. Troponin I and troponin T interact with troponin C to produce different $Ca^{2+}$-dependent effects on actin-tropomyosin filament motility. *Biochem. J.* 327:335–340.

40. Driver, J. W., D. K. Jamison, …, M. R. Diehl. 2011. Productive cooperation among processive motors depends inversely on their mechanochemical efficiency. *Biophys. J.* 101:386–395.

41. Bieling, P., I. A. Telley, …, T. Surrey. 2008. Processive kinesins require loose mechanical coupling for efficient collective motility. *EMBO Rep.* 9:1121–1127.

42. Roostalu, J., C. Hentrich, …, T. Surrey. 2011. Directional switching of the kinesin Cin8 through motor coupling. *Science.* 332:94–99.

43. Lipowsky, R., J. Beeg, …, M. Müller. 2010. Cooperative behavior of molecular motors: Cargo transport and traffic phenomena. *Physica E.* 42:649–661.

44. Klumpp, S., and R. Lipowsky. 2005. Cooperative cargo transport by several molecular motors. *Proc. Natl. Acad. Sci. USA.* 102:17284–17289.

45. Beeg, J., S. Klumpp, …, R. Lipowsky. 2008. Transport of beads by several kinesin motors. *Biophys. J.* 94:532–541.

46. Li, X., R. Lipowsky, and J. Kierfeld. 2013. Bifurcation of velocity distributions in cooperative transport of filaments by fast and slow motors. *Biophys. J.* 104:666–676.

47. Debold, E. P., J. B. Patlak, and D. M. Warshaw. 2005. Slip sliding away: load-dependence of velocity generated by skeletal muscle myosin molecules in the laser trap. *Biophys. J.* 89:L34–L36.

48. Badoual, M., F. Jülicher, and J. Prost. 2002. Bidirectional cooperative motion of molecular motors. *Proc. Natl. Acad. Sci. USA.* 99:6696–6701.

49. Li, X., R. Lipowsky, and J. Kierfeld. 2012. Critical motor number for fractional steps of cytoskeletal filaments in gliding assays. *PLoS ONE.* 7:e43219.

50. Hartigan, J., and P. Hartigan. 1985. The dip test of unimodality. *Ann. Stat.* 13:70–84.